Journal of Magnetic Resonance 199 (2009) 214–224

Contents lists available at ScienceDirect

Journal of Magnetic Resonance

journal homepage: www.elsevier.com/locate/jmr

Generalized MAGSTE with bipolar diffusion-weighting gradient pulses

Jürgen Finsterbusch *

Department of Systems Neuroscience, University Medical Center Hamburg-Eppendorf, Hamburg, Germany
Neuroimage Nord, University Medical Centers Hamburg–Kiel–Lübeck, Germany

ARTICLE INFO

Article history:
Received 23 January 2009
Revised 8 May 2009
Available online 13 May 2009

Keywords:
Background gradients
Cross-term compensation
MRI
Diffusion
Generalized MAGSTE
Bipolar gradients

ABSTRACT

The generalized magic asymmetric gradient stimulated echo (generalized MAGSTE) sequence compensates background gradient cross-terms and can be adjusted to asymmetric timing boundary conditions which for instance are present in echo-planar MR imaging. However, its efficiency is not optimal because one of the two diffusion-weighting gradients applied in each interval usually must have a reduced amplitude to ensure the desired cross-term compensation. In this work, a modification of generalized MAGSTE is investigated where this gradient pulse is replaced by two gradient pulses with full amplitude but opposite polarities. It is shown that with these bipolar gradients (i) the sequence retains the cross-term compensation capability for an appropriate choice of the gradient pulse durations and (ii) the diffusion-weighting efficiency is improved, i.e. higher k and b values can be achieved without prolonging the echo time. These results are confirmed in MR imaging experiments on phantoms and in vivo in the human brain at 3 T using spin-echo and echo-planar MR imaging. In the examples shown, the b value could be increased between about 30% and 200% when using the bipolar gradient pulses. Thus, bipolar gradients may help to improve the applicability of the generalized MAGSTE sequence.

1. Introduction

The measurement of diffusion coefficients with pulsed-field-gradient NMR [1–3] is often hampered by macroscopic or microscopic background gradient fields which are caused by magnetic field inhomogeneities or susceptibility differences in heterogeneous samples [4]. The interaction of these background gradients with the pulsed gradients applied for diffusion weighting results in a so-called cross term (e.g. [5]). The cross-term is proportional to the product of both gradient amplitudes and thus yields a diffusion weighting which neither is constant nor increases with the square of the pulsed gradient amplitude when varying the diffusion-weighting gradients. Consequently, it distorts the expected signal behavior and yields incorrect diffusion coefficients if it is not taken into account appropriately. Whereas the effect of macroscopic background gradients, i.e. those that can be considered to be constant within the measurement volume or across a voxel, vanishes when taking the geometric mean of acquisitions with opposite polarities of the diffusion-weighting gradient pulses, microscopic gradient fields, i.e. those that vary on a length scale well below the measurement volume or voxel size, are inert to this approach.

Thus, pulse sequences which inherently null these cross-terms in each acquisition have been developed in the past. They involve a modified switching of the pulsed gradients in combination with additional RF pulses. For the standard spin-echo diffusion-weighting preparation, it has been shown that the use of multiple refocusing RF pulses is sufficient to compensate the cross-terms [6]. Analogously, the pulsed-gradient stimulated echo (PGSTE) preparation that is the gold standard for samples with a T_2 relaxation time short compared to the desired diffusion time, has been extended by applying refocusing RF pulses in the middle of the preparation and readout interval and two gradient pulses of opposite polarity for the diffusion weighting in each of the intervals [7]. However, this approach presented by Cotts et al. cannot compensate cross-terms of background gradient fields that change during the middle interval of the stimulated echo, i.e. if the diffusing spins "feel" different background gradient fields in the preparation and readout interval. Because long diffusion times can be achieved with the PGSTE preparation, this is a rather common scenario in heterogeneous samples (e.g. [8]).

As a solution, the so-called magic asymmetric gradient stimulated echo (MAGSTE) sequence has been developed [9–12]. It compensates cross-terms in the readout and preparation interval independently by using a certain, so-called "magic" ratio of the amplitudes of the two pulsed gradients in each interval.

Several extensions of the MAGSTE sequence have been presented to improve its performance. In the first, a third gradient pulse of inverted polarity is introduced which yields an increased

* Address: Institut für Systemische Neurowissenschaften, Geb. W34, Universitätsklinikum Hamburg-Eppendorf, 20246 Hamburg, Germany. Fax: +49 40 7410 59955.
E-mail address: j.finsterbusch@uke.uni-hamburg.de.

1090-7807/$ - see front matter © 2009 Elsevier Inc. All rights reserved.
doi:10.1016/j.jmr.2009.05.004

diffusion-weighting efficiency [13]. Thereby, the assumption of identical delay times at the begin and end of each interval that is present in most non-imaging experiments, was retained. Another, the so-called generalized MAGSTE sequence, focusses on imaging experiments and is a modification that takes asymmetric timing demands as in diffusion-weighted echo-planar imaging (EPI) [15] into account, i.e. different delay times at the begin and end of the readout interval. It extends the standard MAGSTE experiment by using different durations for the two diffusion-weighting gradient pulses in the interval in order to cover all the time available and improve the diffusion-weighting efficiency accordingly. Most recently, a modification has been presented that involves additional refocusing RF pulses in the readout and preparation interval to shorten the echo times of the individual spin echoes involved and thus reduce the sensitivity to background gradient fields that vary within the preparation or readout interval [16].

In this work, the idea of using bipolar diffusion-weighting gradient pulses in MAGSTE sequences [13], so far considered and investigated only for identical delay times, is applied to generalized MAGSTE in order to achieve a further improvement of the diffusion-weighting efficiency for imaging experiments. The gradient pulse with the lower amplitude is replaced by a combination of two gradient pulses with full amplitude but opposite polarities. It is shown theoretically and experimentally that (i) the pulse durations can be adjusted to ensure the cross-term compensation in the preparation and readout interval independently and (ii) higher k and b values can be achieved without prolonging the echo time, i.e. the diffusion-weighting efficiency is improved.

2. Theory

In Fig. 1a, the basic MAGSTE pulse sequence is shown. If the gradient pulse amplitudes obey the, so-called "magic", ratio [9,11]

$$|\eta| = \frac{\delta^2 + 3\delta\delta_1 + 3\delta_1^2}{5\delta^2 + 9\delta\delta_1 + 3\delta_1^2 + 12(\delta + \delta_1)\delta_2 + 6\delta_2^2} \tag{1}$$

cross-terms with background gradient fields are nulled in the preparation and readout interval independently.

In general, the times required for the individual RF excitations and/or the data acquisition may differ. For instance, the time needed for the echo train of diffusion-weighted EPI may exceed that for the $\pi/2$ RF excitation in the readout interval considerably (e.g. see Fig. 1). A similar difference can be present in the preparation interval, e.g. when using long RF pulses like 2D-selective RF (2DRF) excitations [17–19] for the initial RF excitation. Thus, an asymmetric timing of the two diffusion-weighting gradient pulses in each interval can be helpful to avoid unused fill times and reduce the echo time.

An example of this generalized MAGSTE sequence is shown in Fig. 1b for a long data acquisition part, e.g. required for the echo train of an EPI acquisition ("Read" direction in Fig. 1g). Compared to the standard MAGSTE sequence it involves a shorter delay time δ_3 and a longer gradient pulse of duration δ' in the first part of the readout interval. In the example shown, both gradient pulses have identical amplitudes, i.e. the "magic" amplitude ratio of the MAGSTE sequence has changed to a "magic" duration ratio. However, with the boundary condition of cross-term compensation this special case only occurs if [14]

$$\delta_{3,\mathrm{magic}} = \sqrt[3]{\delta_1^3 - (6\delta_2 + 12\delta_1)\delta_2\,\delta - (6\delta_1 + 12\delta_2)\,\delta^2 - 4\delta^3}. \tag{2}$$

For arbitrary δ_3, a modified gradient pulse amplitude ratio η' is required to ensure the compensation which is given by [14]

$$\eta' = \frac{g_1}{g_2} = \frac{\delta^3 + 3\delta_1\,\delta^2 + 3\delta_1^2\,\delta + \delta_1^3 - \delta_3^3}{\delta\left(5\,\delta^2 + (9\delta_1 + 12\delta_2)\,\delta + 3\delta_1^2 + 12\delta_1\delta_2 + 6\delta_2^2\right)}. \tag{3}$$

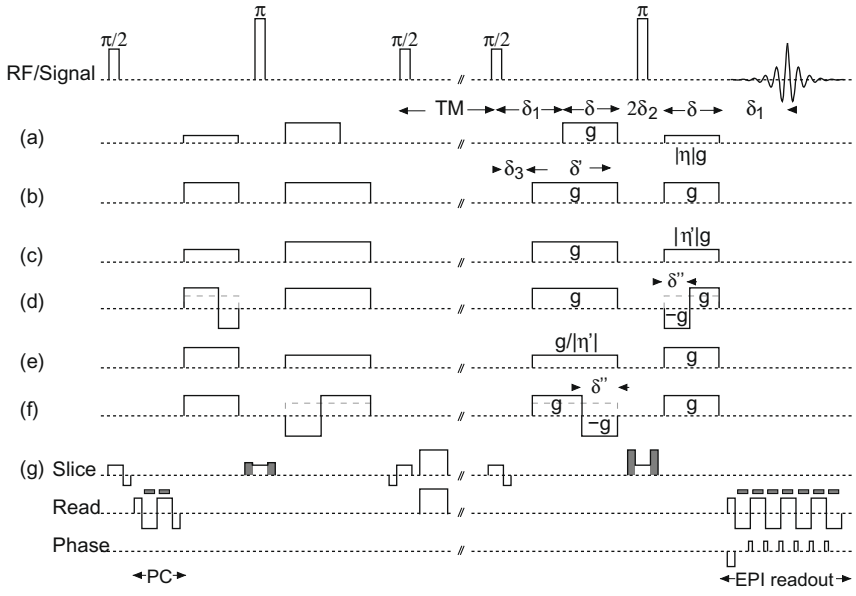

Fig. 1. Basic RF (upper) and gradient pulse sequences of (a) standard MAGSTE and generalized MAGSTE with (b, c, and e) monopolar diffusion-weighting gradient pulses, i.e. as presented previously, and (d and f) with bipolar diffusion-weighting gradient pulses. In (b) identical amplitudes of the two gradient pulses are assumed, i.e. the special case where the gradient pulses differ only by their length is shown which is achieved for $\delta_3 = \delta_{3,\mathrm{magic}}$. (c) The timing for the so-called "short-echo-train" regime ($\delta_3 > \delta_{3,\mathrm{magic}}$) where the second gradient pulse in the readout interval has a lower amplitude. (d) The modification where this gradient pulse is replaced by bipolar gradient pulses, i.e. a combination of two gradient pulses with full amplitude but opposite polarity. (e and f) The corresponding sequences for the "long-echo-train" regime, i.e. $\delta_3 < \delta_{3,\mathrm{magic}}$. If δ'' in (d and f) is chosen appropriately, cross-terms with background gradients are compensated as in (b, c, and e). A mirror-symmetric sequence timing is shown in (a–f) but it should be noted that due to the cross-term compensation achieved in each interval independently, preparation and readout intervals with different timings can be combined without sacrificing the cross-term compensation. (g) Basic sequence for the gradient pulses applied for spatial selectivity and encoding in the EPI experiments performed. Seven k-space lines and two non-phase-encoded reference echoes used for phase-correction (PC) are shown. Gray gradient pulses are dedicated to spoil unwanted transverse coherences.

For the magic duration ratio which corresponss to $\eta' = 1$ (Fig. 1b), the diffusion-weighting efficiency is optimal because both gradients in the readout interval have the same (maximum) amplitude. For $\eta' < 1$, the second gradient pulse has the lower amplitude (Fig. 1c). Assuming that the echo train of echo-planar imaging is the reason for $\delta_1 > \delta_3$ and the motivation to apply diffusion gradients with different pulse durations (as shown in Fig. 1), this case can be considered as the "short-echo-train" regime because the echo train, and thus δ_1, is too short to achieve the optimum diffusion-weighting efficiency with $\eta' = 1$. For $\delta_1 = \delta_3$, which will not be considered in detail here, the short-echo-train regime reduces to a previously described modification of the MAGSTE sequence [13]. If $\eta' > 1$, the first gradient pulse in the readout interval has the lower amplitude (Fig. 1e). This represents the "long-echo-train" regime because then the echo train (and δ_1) is too long to achieve the optimum efficiency.

In both cases, the gradient pulses with the lower amplitude can be replaced by bipolar gradient pulses, i.e. a combination of two gradient pulses with the full amplitude but opposite polarities. Thus, the pulse sequences shown in Fig. 1d and f are obtained for the short- and long-echo-train regime, respectively. It will be shown that for both regimes (i) the cross-term compensation can be retained if the pulse durations are chosen appropriately while (ii) the diffusion-weighting efficiency is improved.

2.1. Short-echo-train regime

Due to the cross-term compensation desired for each of the preparation and readout intervals independently, it is sufficient to consider the preparation interval only. The derived results also hold for the readout interval.

The cross-term of the pulsed gradients shown in Fig. 1d with a constant (background) gradient field g_b is given by

$$\begin{aligned} b_{\text{cross,short}} = \; & \gamma^2 g_b \Big(\tfrac{1}{6}\delta''^3 (g_1+g_2) - \tfrac{1}{2}\delta''^2 (g_1+g_2)(\delta+\delta_1) \\ & - \tfrac{1}{2}\delta'' (g_1+g_2)\left((\delta+\delta_1+2\delta_2)^2 - 2\delta_2^2\right) \\ & + \tfrac{1}{6} g_1 \left(5\delta^3 + \delta^2(9\delta_1+12\delta_2) + \delta\left(6(\delta_1+\delta_2)^2 - 3\delta_1^2\right)\right) \\ & - \tfrac{1}{6} g_2 \left(\delta^3 + \delta_1^3 - \delta_3^3 + 3\delta\delta_1(\delta+\delta_1)\right)\Big) \end{aligned} \tag{4}$$

where γ represents the gyromagnetic ratio and rectangular gradient pulses have been assumed for the sake of simplicity.

The cross-term vanishes if

$$\delta''_{\text{short}} = \delta + \delta_1 - 2\sqrt{2}(\delta+\delta_1+\delta_2)\cos\left[\frac{\pi}{3} + \frac{1}{3}\arccos\left(\frac{6\delta^3 + 11\delta_1^3 - \delta_3^3 + 12(\delta^2+\delta_1\delta_2)(2\delta_1+\delta_2) + 6\delta(5\delta_1^2 + 6\delta_1\delta_2 + \delta_2^2)}{8\sqrt{2}(\delta+\delta_1+\delta_2)^3}\right)\right] \tag{5}$$

which has been obtained according to the method of Cardano [20,21] (see Appendix A). This solution is (i) positive for any $\delta_3 > \delta_{3,\text{magic}}$, i.e. within the complete short-echo-train regime, and (ii) lower than δ for $\delta_3 \leqslant \delta + \delta_1$, i.e. for any $\delta' > 0$ (see Appendix A). Thus, it ensures that the desired cross-term compensation can be achieved for any timing parameters within the short-echo-train regime. For $\delta_1 = \delta_3$, i.e. symmetric delay times, the solution simplifies to that described in [13] as expected.

Because the gradient pulse duration in real experiments usually must meet some raster time (i.e. the dwell time of the gradient waveform), Eq. (5) may be of limited value for practical purposes. However, different amplitudes can be used for the diffusion-weighting gradient pulses to ensure that the cross-terms are compensated for the δ'' rounded to the gradient raster time. Solving $b_{\text{cross,short}} = 0$ yields

$$\begin{aligned} & g_1 \left(-2\delta''^3 + 6\delta''^2(\delta+\delta_1) + 6\delta''((\delta+\delta_1+2\delta_2)^2 - 2\delta_2^2) - 10\delta^3 \right. \\ & \left. -6\delta^2(3\delta_1+4\delta_2) - 6\delta(\delta_1^2 + 4\delta_1\delta_2 + 2\delta_2^2)\right) \\ & = g_2 \left(2\delta''^3 - 6\delta''^2(\delta+\delta_1) - 6\delta''\left((\delta+\delta_1+2\delta_2)^2 - 2\delta_2^2\right) - 2\delta^3 \right. \\ & \left. -2\delta_1^3 + 2\delta_3^3 - 6\delta\delta_1(\delta+\delta_1)\right) \end{aligned} \tag{6}$$

which can be used to scale the gradient pulse amplitudes for any given δ''. Thereby, g_1 represents the amplitude for the first gradient pulse in the preparation interval (or the last gradient pulse in the readout interval) while g_2 and $-g_2$ are to be used for the other two gradient pulses, respectively.

Considering the gradient integrals k, it can be shown that with bipolar gradient pulses higher k values are obtained (see Appendix B), i.e. the diffusion-weighting efficiency is improved with respect to k. A corresponding analysis for the b value is difficult and could not be obtained due to the complex equations but numerical simulations were performed (see below).

2.2. Long-echo-train regime

For the long-echo-train regime, i.e. the pulse sequence of Fig. 1f, the cross-term for rectangular diffusion-weighting gradient pulses is given by

$$\begin{aligned} b_{\text{cross,long}} = \gamma^2 g_b \Big(& \frac{1}{6}\delta''^3 (g_1+g_2) - \frac{1}{2}\delta''^2 (g_1+g_2)(\delta+\delta_1) \\ & + \frac{1}{2}\delta''(g_1+g_2)(\delta+\delta_1)^2 + \frac{1}{6} g_1 \left(5\delta^3 + \delta^2(9\delta_1+6\delta_2)\right. \\ & \left. + 3\delta(\delta_1^2 + 4\delta_1\delta_2 + 2\delta_2^2)\right) \\ & - \frac{1}{6} g_2 \left(\delta^3 + \delta_1^3 - \delta_3^3 + 3\delta\delta_1(\delta+\delta_1)\right)\Big). \end{aligned} \tag{7}$$

The zero-crossing of this expression is (see Appendix A)

$$\delta''_{\text{long}} = \delta + \delta_1 - \frac{1}{2}\sqrt[3]{4\delta_3^3 + 24\delta^3 + 4\delta_1^3 + 48\delta^2(\delta_1+\delta_2) + 24\delta(\delta_1+\delta_2)^2} \tag{8}$$

which for $\delta_3 \leqslant \delta + \delta_1$, i.e. the boundary condition of the long-echo-train regime, is (i) positive and (ii) lower than $\delta + \delta_1 - \delta_3$, i.e. lower than δ' (see Appendix A). Thus, it is a reasonable solution and ensures compensation of cross-terms for the complete parameter range of the long-echo-train regime.

Because Eq. (8) may also yield a pulse duration that is not on the required gradient raster time, the amplitudes of the gradient pulses can be adjusted to retain the cross-term compensation according to

$$\begin{aligned} & g_1 \left(-2\delta''^3 + 6\delta''^2(\delta+\delta_1) - 6\delta''(\delta+\delta_1)^2 - 10\delta^3 - 6\delta^2(3\delta_1+4\delta_2) \right. \\ & \left. -6\delta(\delta_1^2 + 4\delta_1\delta_2 + 2\delta_2^2)\right) \\ & = g_2 \left(2\delta''^3 - 6\delta''^2(\delta+\delta_1) + 6\delta''(\delta+\delta_1)^2 - 2\delta^3 - 2\delta_1^3 + 2\delta_3^3 \right. \\ & \left. -6\delta\delta_1(\delta+\delta_1)\right) \end{aligned} \tag{9}$$

for any δ''. Here, g_2 is the amplitude of the last gradient pulse in the preparation interval (or the first gradient pulse in the readout interval) while $-g_1$ and g_1 are the amplitudes of the other two gradient pulses, respectively.

As for the short-echo-train regime, the gradient integral k achieved with bipolar gradients is higher for a given timing (see Appendix A). To investigate the b efficiency, numerical simulations were required (see below).

2.3. Finite ramp times

In practice, finite ramp times, i.e. trapezoidal gradient pulses, must be used. Eq. (5) and (8) could be extended accordingly but would represent only a part of the solution because pulse durations on the gradient raster time are required. Thus, it is easier to use the pulse durations δ'' of Eqs. (5) and (8), respectively, round it to the gradient raster time, and adjust the gradient pulse amplitudes according to the extensions of Eqs. (6) and (9) for finite ramp times which can be calculated straightforwardly and are given in Appendix C. This approach was used in the present study.

2.4. Asymmetric timing

In some experiments, an asymmetric timing with different fill times δ_2 and δ_2' prior to and after the refocusing RF pulse, respectively, may be required. The solutions obtained for δ'' in this case are provided in Appendix D.

3. Experimental

The analytical derivations leading to Eqs. (4)–(9) and the numerical calculations for the plots shown were obtained with Maple 10 (version May 13 2005, Waterloo Maple Inc., Waterloo, Ontario, Canada). Numerical calculations of the k and b values in the preparation interval were performed in IDL (version 5.5a, Research Systems Inc., Boulder, CO, USA). Thereby, δ was varied between 0.2 ms and 50.0 ms, δ_1 between 0.2 ms and 100.0 ms, δ_2 between 0.2 ms and 20.0 ms, and δ_3 between 0.2 ms and the minimum of δ_1 and 30.0 ms, all in steps of 0.2 ms.

MR measurements were performed on a 3 T whole-body MR system (Magnetom Trio, Siemens Healthcare, Erlangen, Germany). The RF was transmitted via the body coil while a standard 12-channel head coil was used for signal reception. Water phantoms, a cantaloupe (*cucumis melo reticulatus*) and healthy volunteers were investigated. From the latter, informed consent was obtained prior to the examination according to the institution's guidelines.

The diffusion-weighting preparations shown in Fig. 1b–f and the preparation of Cotts et al. [7] as well as a standard PGSTE preparation were combined with an EPI sequence (Fig. 1g) as described previously [14] and a standard spin-echo sequence. For the spin-echo sequence, the gradient pulses and data acquisitions related to phase correction (PC in Fig. 1g) were discarded. Furthermore, only a single echo per shot was acquired in the readout interval which was preceded by a standard (warp) phase-encoding gradient pulse. To mimic the effect of background gradients, two additional pulsed gradients in slice direction which covered the full preparation and readout interval, respectively, could be inserted into the different preparation sequences with independently user-selectable amplitudes.

MR images were acquired with an in-plane resolution of $3 \times 3\ mm^2$, a slice thickness of 10 mm in phantoms and 5 mm *in vivo*, respectively, and a repetition time (TR) of 12,000 ms in phantoms and 6000 ms *in vivo*, respectively. Standard spin-echo MR images were obtained with a receiver bandwidth of 260 Hz per pixel and a field-of-view of $180 \times 240\ mm^2$ yielding an acquisition time of 12 min per image. For acquisitions with 2DRF excitations the field-of-view in the phase-encoding direction could be reduced to 36 mm plus 15 mm oversampling (3 min 24 s per image) without aliasing. Echo-planar images were acquired with field-of-views of $180 \times 240\ mm^2$ in phantoms and $192 \times 240\ mm^2$ *in vivo*, respectively. The receiver bandwidth was 1785 Hz per pixel in phantoms and 1840 Hz per pixel *in vivo*, respectively. Thus, identical echo times could be obtained in phantom and *in vivo* experiments.

2DRF excitations were calculated according to the low-flip-angle approximation [18]. The blipped-planar trajectory had a resolution of $10 \times 10\ mm^2$ and a field-of-excitation, i.e. a distance of the periodic side excitations, of 150 mm yielding 15 k-space lines (total duration 5.7 ms). The desired excitation volume was a rectangular profile with a size of $10 \times 42\ mm^2$ (slice $\times$ phase-encoding direction). To reduce ringing artifacts, the RF envelope was multiplied with a two-dimensional Gaussian filter which achieved 15% of its maximum intensity at the extreme k-space coordinates. 2DRF pulses were scaled to yield a flip angle of 90°.

Diffusion weighting was performed either in slice direction only (spin-echo imaging) or in phase, read, and slice direction (EPI). Mixing times (TM) of 150 ms or 300 ms were used, b values were 500, 1000, 1500, and 2000 s mm^{-2} for spin-echo imaging and 500 and 1500 s mm^{-2} for EPI measurements, respectively. To demonstrate the improved diffusion-weighting efficiency of the presented extension, some generalized MAGSTE acquisitions with monopolar gradients were performed with the same gradient pulse magnitudes as with bipolar gradient pulses which yielded lower b values (see below). For the PGSTE preparation, the echo time was 71 ms. EPI acquisitions with generalized MAGSTE were performed with echo times between 119 ms and 128 ms, those with the standard MAGSTE preparation [9] with about 220 ms, respectively. Spin-echo images were obtained with echo times between 81 ms and 90 ms for generalized MAGSTE, for standard MAGSTE 102 ms were required.

To demonstrate the cross-term compensation capability of generalized MAGSTE with bipolar diffusion-weighting gradient pulses, measurements of the apparent diffusion coefficient (ADC) on a water phantom were performed where background gradient fields were mimicked by switching pulsed gradients. In contrast to microscopic background gradient fields that cause a phase distribution and a related magnitude reduction of the magnetization in each voxel, these macroscopic gradient fields yield a phase modulation on a macroscopic scale, i.e. distort the magnetization's phase in each voxel differently. This modulation can cause additional artifacts in echo-planar imaging. Thus, these acquisitions were performed with spin-echo imaging but timing parameters (durations of diffusion-weighting gradient pulses) were chosen to match that of the corresponding EPI acquisitions and an echo time of 120 ms was used.

The ADC was calculated on a voxel-by-voxel basis with software provided by the manufacturer (syngo MR, VB15). The ADC values reported represent the mean value observed in a region-of-interest in the central part of the phantom.

4. Results

Fig. 2 shows examples of the time courses for trapezoidal gradients (Fig. 2a), their time integral (Fig. 2b), their b value (Fig. 2c), and their cross-term with a constant background gradient (Fig. 2d) for both echo-train regimes in comparison to the generalized MAGSTE sequence with monopolar gradient pulses (gray lines). For the sake of clarity, only the preparation interval is shown. To yield the time courses for the readout interval, the plot of the gradients (Fig. 2a), their time integral (Fig. 2b) and the

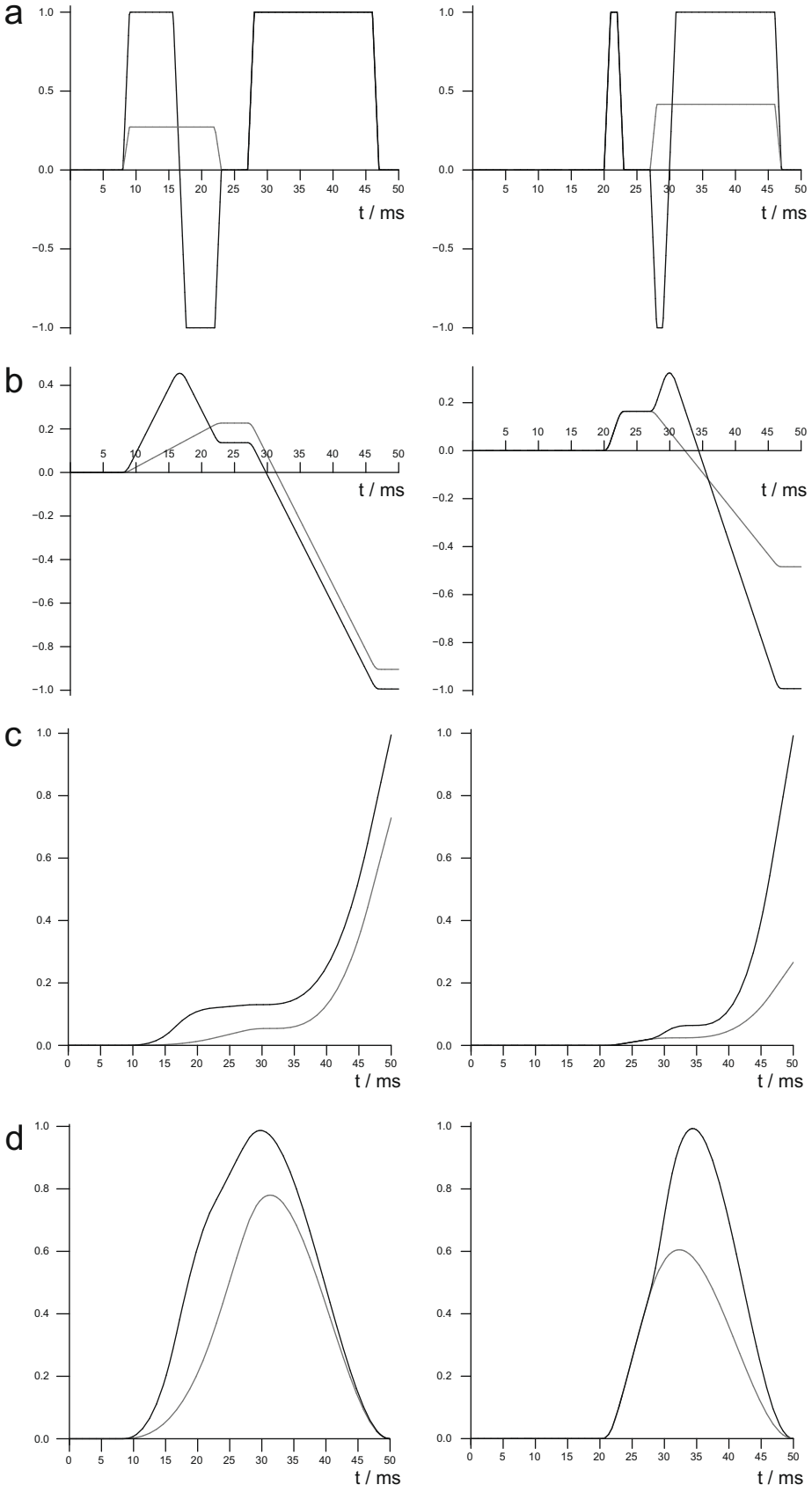

Fig. 2. Example time courses (in ms) in the preparation interval for generalized MAGSTE with monopolar (gray) and bipolar diffusion-weighting gradient pulses (black) showing (a) the diffusion-weighting gradient pulses, (b) their time integral, i.e. *k* values, (c) their *b* value, and (d) their cross-terms with a constant background gradient for the short-echo-train (left) and the long-echo-train time regime (right), respectively. In both examples, δ_2 and δ_3 were 3 ms, the ramp time 1 ms. For the short-echo-train example a δ of 14 ms and a δ_1 of 8 ms were used, for the long-echo-train example 2 ms and 20 ms, respectively. The refocusing RF pulse is applied at 25 ms. The ordinates are in arbitrary units.

cross-term (Fig. 2d) must be reversed along the time axis. The plots of the *b* values (Fig. 2c) need to be mirrored along the time and the *b* axis to obtain the readout interval time course such that the curves approach their maximum value at the end of the interval.

In the short-echo-train example, the first gradient needs to be replaced by the bipolar gradients. The gain in *k* and *b* compared to generalized MAGSTE is only about 10% and 20%, respectively. This is because the additional integral introduced by the second (negative) gradient pulse is small compared to that of the gradient in the second half of the preparation interval. However, for typical EPI acquisitions, the long-echo-train regime is more relevant. The corresponding example shows that the last gradient in the preparation interval is slightly shortened for the bipolar gradients but also has a clearly higher amplitude. This causes a steeper slope in the *k* plots (Fig. 2b) which yields considerably increased *k* values (about a factor of 2) at the end of the integral although the "break-even" point with the preceding gradients of effectively opposite polarities, i.e. the zero-crossing, is achieved later. For the *b* values achieved within the preparation interval (Fig. 2c), the gain is even higher with a factor of about 4. This improvement can also be expected when taking the TM interval into account because the *b* value in this interval increases with the k^2 at the end of the preparation interval. In both examples, the cross-term with the background gradient vanishes as expected at the end of the interval which is also observed for the generalized MAGSTE sequence (Fig. 2d).

The numerical calculations revealed that the *k* values achieved in the preparation interval with bipolar gradients are superior to those of the generalized MAGSTE sequence which is consistent with the theoretical considerations performed. For the *b* values of the preparation interval some combinations of δ and the δ_i could be found that yield slightly (about 0.3%) lower values for the proposed extension. These values were obtained for a short δ (about 0.8 ms), a δ_2 of 0.2 ms, and $\delta_3 \approx \delta_1 \approx 30.0$ ms. Most likely, the values below 1 occur due to rounding errors as they coincide with very short δ'' of 0.06 ms or below. But even if the values are correct, it should be emphasized that this reduction refers to the *b* value of the preparation or readout interval alone and can be compensated by the *b* contribution achieved during TM which is proportional to k^2. For the range of parameters used in the calculations a TM as short as 18 ms is sufficient to obtain higher *b* values than with the generalized MAGSTE sequence. Because stimulated echo preparations are preferred for long diffusion times, it is unlikely that shorter TM values are relevant in practice.

In Fig. 3, values of δ'' compared to δ and δ' are presented for the short-echo-train (Fig. 3a) and the long-echo-train regime (Fig. 3b), respectively. Typically, δ'' is about 20–40% of δ for the short-echo-train regime (Fig. 3a) which also is observed in Fig. 2a. It

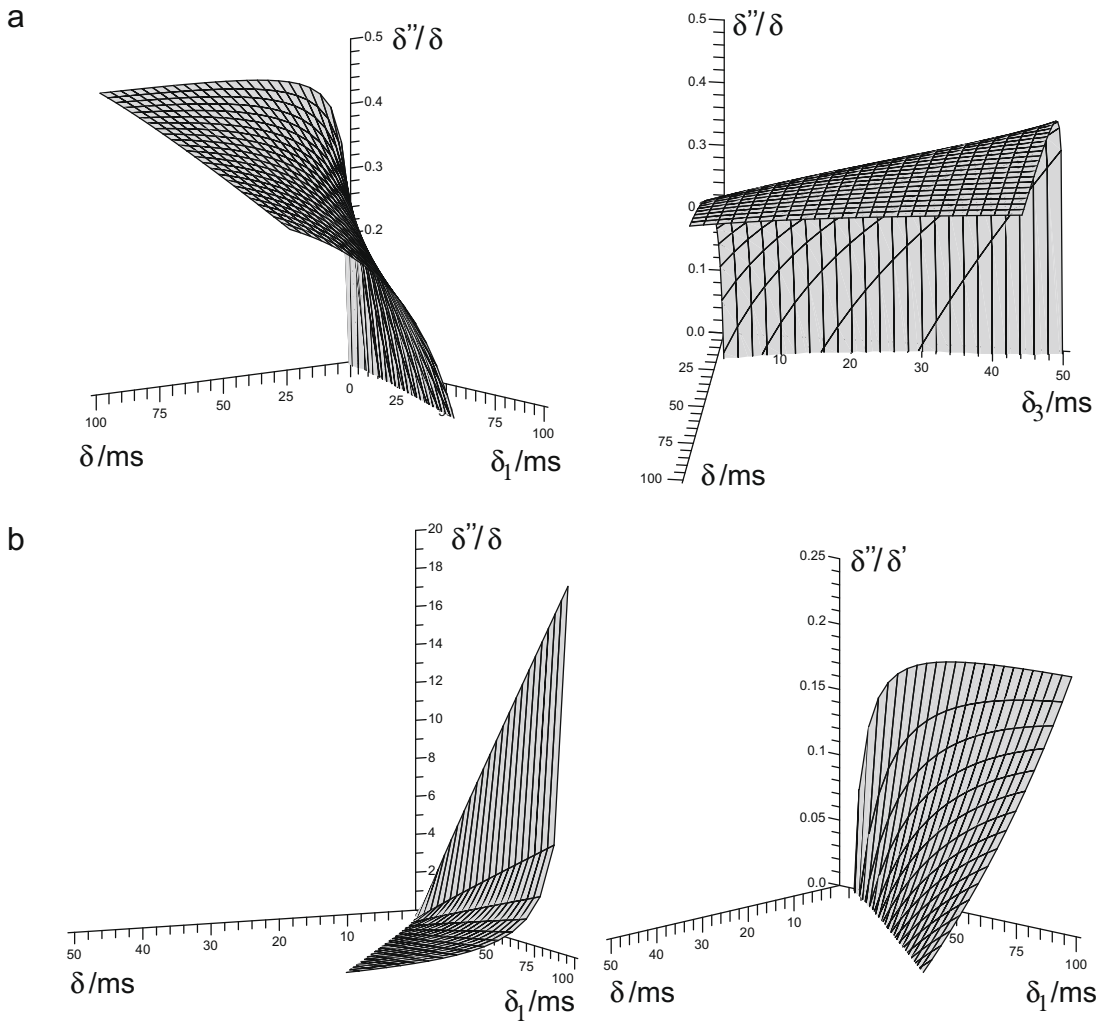

Fig. 3. δ'' relative to δ and δ', respectively, for (a) the short-echo-train and (b) the long-echo-train regime vs. δ_1 and δ_3, respectively, and δ. A gradient ramp time of 1 ms was used in all plots. $\delta_2 = \delta_3$ was assumed and set to 3 ms if δ_3 was not one of the abscissas.

approaches zero for $\delta_3 = \delta_{3,\mathrm{magic}}$ which defines the case that both gradient pulses in the generalized MAGSTE sequence with monopolar gradient pulses have identical amplitudes, i.e. the efficiency is already optimal and cannot be further improved by the use of bipolar gradient pulses. For the long-echo-train regime (Fig. 3b), δ'' can be much larger than δ because it now represents a fraction of the time δ' available for the diffusion gradients prior to the refocusing RF in the readout interval. Compared to δ', it typically is about 10–20% and also approaches zero for $\delta_3 = \delta_{3,\mathrm{magic}}$ as expected.

Plots of the k and b values achieved with bipolar gradient pulses relative to those obtained with monopolar gradient pulses are presented in Fig. 4. For the short-echo-train regime (Fig. 4a) typical k ratios are about 1.1. Accordingly, the b value gain for long TM (500 ms) is about 20%. It increases when shortening TM, up to 30–60% for 10 ms. This difference is due to the additional contribution to b caused by the intermediate de- and rephasing within the preparation that is not reflected in the k value achieved at the end of the interval. Thus, it is independent of TM and appears more pronounced if the contribution related to TM which is proportional $k^2 \cdot \mathrm{TM}$ is small.

The gains are much more pronounced in the long-echo-train regime (Fig. 4b), in particular for shorter δ and longer δ_1. k^2 and b values may be several times higher compared to generalized MAGSTE. The b ratio shows some dependency on TM (data not shown) but the differences are marginal relative to the values of Fig. 4b. As expected, all plots approach 1 for $\delta_3 = \delta_{3,\mathrm{magic}}$.

In Fig. 5, ADC maps are shown that were obtained in the water phantom without and with simulated background gradient fields to demonstrate the cross-term compensation capability of generalized MAGSTE with bipolar gradient pulses. Without background gradient fields, ADC values are very similar to those observed previously [14] and range from 1.943 (Fig. 5a) to $1.981 \cdot 10^{-3}\,\mathrm{mm^2\,s^{-1}}$ (Fig. 5c). Compared to the value of about $2.03 \cdot 10^{-3}\,\mathrm{mm^2\,s^{-1}}$ expected for the temperature within the MR room (about 20 °C) [22] a slight but systematic underestimation seems to be present which most likely is caused by an imperfect gradient scaling [14]. A deviation as low as about 2% from the nominal amplitude would be sufficient to induce the observed differences. Applying simulated background gradient fields with 1.0 mT $\mathrm{m^{-1}}$ in both intervals yields already a considerably increased ADC value of $2.23 \cdot 10^{-3}\,\mathrm{mm^2\ s^{-1}}$ (+15%) for the PGSTE preparation (Fig. 5e). Applying different gradient amplitudes in the preparation and readout interval, dephases the STE signal and does not yield images suitable for an ADC calculation (data not shown). In contrast, ADC maps for the other preparations could be calculated when using background gradient amplitudes of −1.0 and +2.0 mT $\mathrm{m^{-1}}$ (Fig. 5f–h). While the preparation of Cotts et al. then yields about

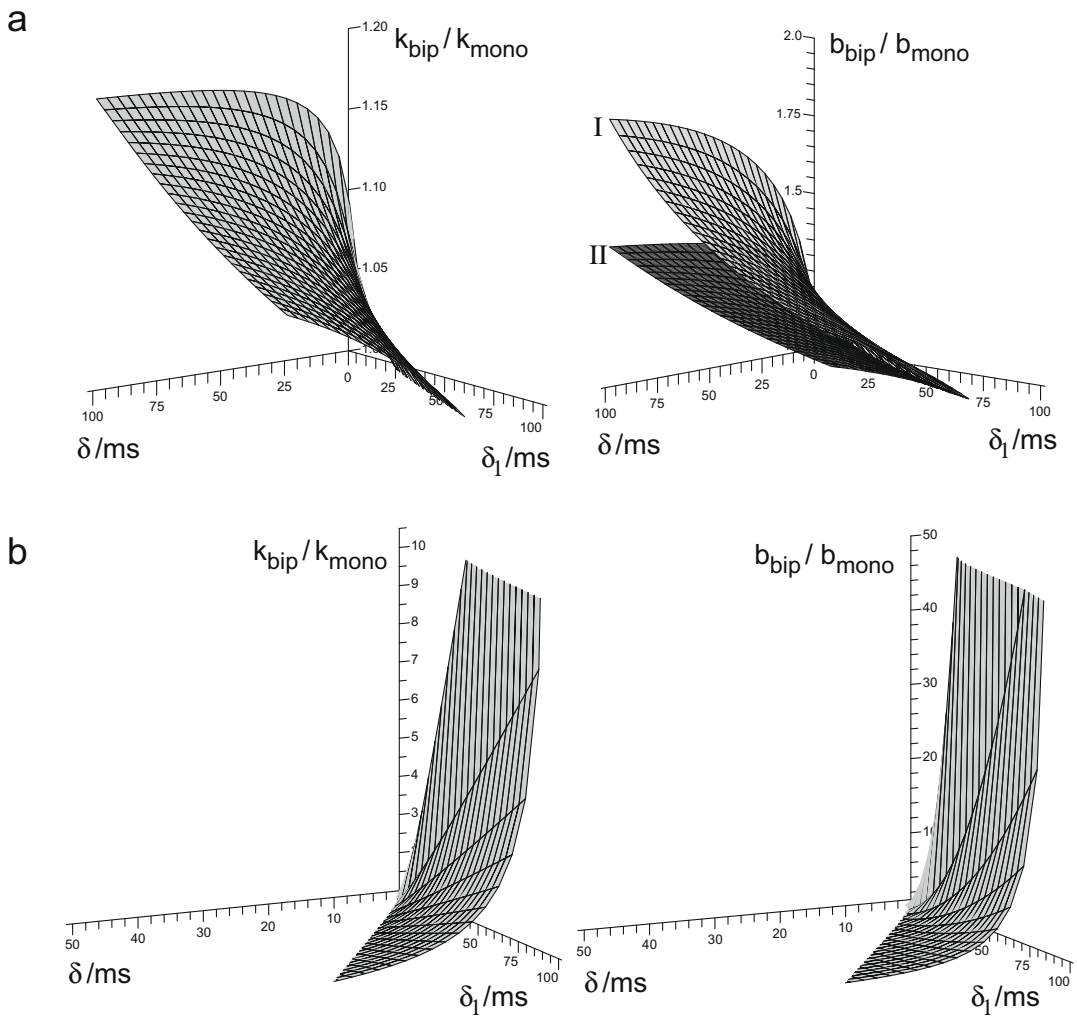

Fig. 4. Relative k (left) and b values (right) of generalized MAGSTE with bipolar compared to monopolar diffusion-weighting gradient pulses for (a) the short- and (b) the long-echo-train regime. For the short-echo-train regime the b values are shown for TMs of 10 ms (I, light gray) and 500 ms (II, dark gray), for the long-echo-train regime b values were calculated for a TM of 300 ms. δ_2 and δ_3 were 3 ms, the gradient ramp time 1 ms in all plots.

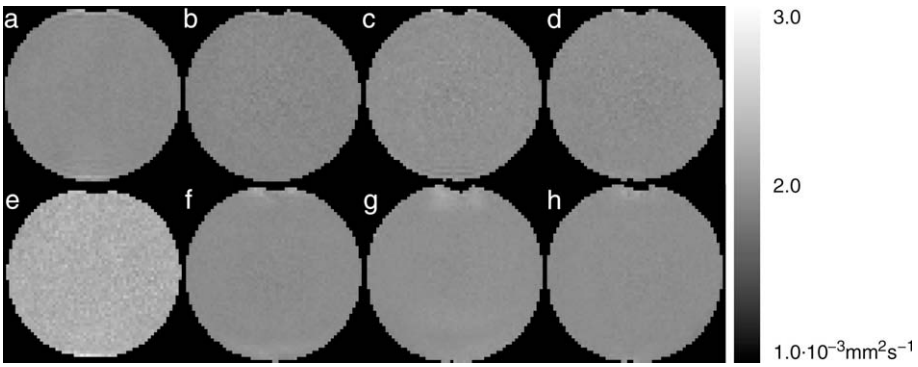

Fig. 5. Maps of the apparent diffusion coefficient (ADC) obtained in a water phantom with (a and e) the standard PGSTE preparation, (b and f) the diffusion preparation of Cotts et al., and generalized MAGSTE with bipolar gradients in (c and g) the short-echo-train and (d and h) the long-echo-train regime, respectively. (e–h) Were acquired with additional gradients to simulate the effect of background gradient fields. For details see text.

2.8% higher ADC values, both generalized MAGSTE preparations showed only a variation of about 0.26% or below which is on the order of the reproducability [14]. This demonstrates the cross-term compensation capability of the generalized MAGSTE preparation with bipolar gradient pulses.

Fig. 6 shows the improved efficiency of generalized MAGSTE with bipolar gradients in the short-echo-train regime. The images of inner-field-of-views were obtained with spin-echo acquisitions using 2DRF excitations in a water phantom and a cantaloupe. Using bipolar diffusion-weighting gradient pulses (Fig. 6a and b) yields significant higher signal attenuations than generalized MAGSTE with monopolar gradient pulses (Fig. 6c and d). In the example shown, the b value in Fig. 6c and d is reduced by about 30% compared to that of Fig. 6a and b. Adapting generalized MAGSTE with monopolar gradient pulses to the same b value requires prolongation of the echo time by about 9 ms (Fig. 6e and f) which yields a signal loss of about 20% in the cantaloupe. In standard MAGSTE (Fig. 6g and h), this loss is more pronounced because the echo time needs to be increased by another 12 ms. Due to the long T_2 relaxation time of water, no such signal difference is obvious in the water phantom.

Corresponding results for the long-echo-train regime and EPI acquisitions are shown in Fig. 7. Comparing generalized MAGSTE with bipolar (Fig. 7a and e) and monopolar (Fig. 7b and f) diffusion-weighting gradient pulses with identical δ clearly shows the higher diffusion-weighting achieved with the presented extension (b value increased by about 100%). To achieve an identical b value, the gradient pulse duration needs to be prolonged which yields a 10% signal loss in brain white matter for generalized MAGSTE with monopolar gradient pulses (Fig. 7c and g) and about 60% for standard MAGSTE (Fig. 7d and h).

5. Discussion

A modification of the generalized MAGSTE sequence is proposed where one of the diffusion-weighting gradient pulses is replaced by bipolar gradient pulses, i.e. a combination of two gradient pulses with full amplitude but opposite polarities. It is applicable to any timing boundary conditions with the exception of the magic length condition where generalized MAGSTE with monopolar diffusion-weighting gradient pulses yields identical amplitudes for both gradient pulses. Beyond this condition and depending on the timing parameters, two regimes can be distinguished which differ by the gradient pulse that yields the lower amplitude and is replaced by the bipolar gradient pulses. For both timing regimes solutions for the gradient pulse durations are provided that retain the cross-term compensation capability of the sequence which applies to the preparation and readout interval independently. The extension with bipolar gradient pulses yields higher k and b values for both timing regimes as has been revealed analytically and with numerical calculations and has been demonstrated experimentally.

Regarding the pulse sequences shown in Fig. 1, it should be kept in mind that different timings can be used in the preparation and readout interval. For instance, if a long echo train in an EPI acquisitions requires a long readout interval with a pronounced timing

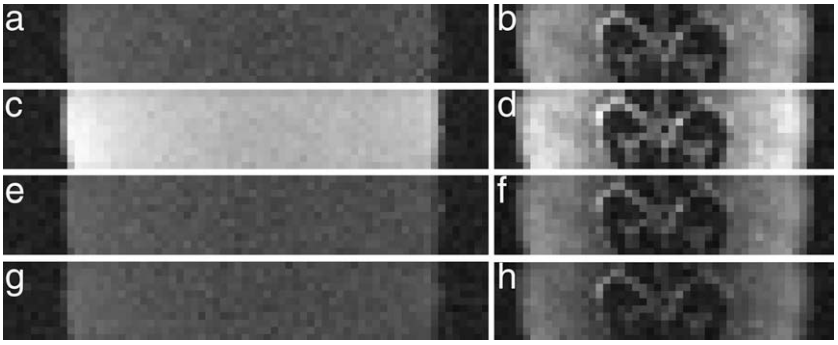

Fig. 6. Diffusion-weighted images of inner field-of-view obtained with a spin-echo sequence (TM 150 ms) and 2DRF excitations using (a–f) generalized MAGSTE and (g and h) standard MAGSTE in (a, c, e, and g) a water phantom and (b, d, f, and h) a cantaloupe. The timing parameters correspond to the short-echo-train regime of generalized MAGSTE with bipolar gradient pulses (a and b). Using monopolar gradients either yields reduced b values (c and d) or a prolonged echo time with a corresponding signal loss (e and f). The latter is even more pronounced for standard MAGSTE (g and h). All images of the same phantom are shown with identical gray scaling, i.e. intensity differences reflect a lower b value or an increased T_2-related signal loss.

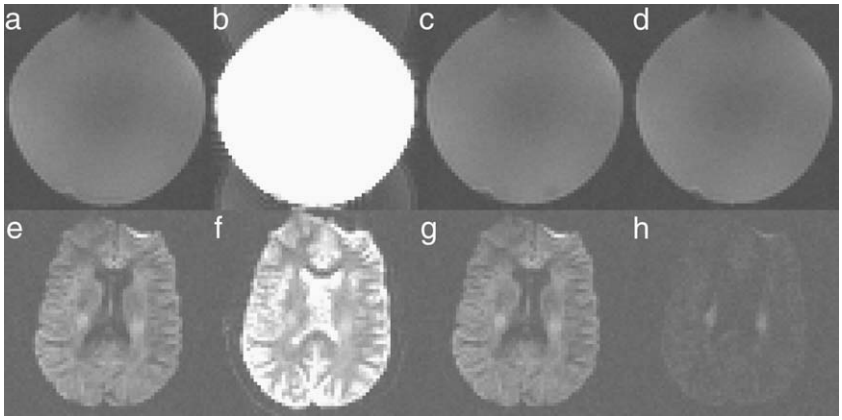

Fig. 7. Diffusion-weighted images acquired with EPI (TM 300 ms) and (a–c, e–g) generalized MAGSTE (long-echo-train regime) and (d and h) standard MAGSTE in (a–d) a water phantom and (e–h) *in vivo*. Generalized MAGSTE with monopolar gradients is at the expense of a reduced *b* value for otherwise identical parameters (b and f) or a signal loss due to a longer echo time (c and g). This also holds for standard MAGSTE with the same *b* value (d and h). All images of the same object are scaled identically, i.e. intensity differences correspond to a reduced *b* value or a lower signal-to-noise ratio.

asymmetry of the diffusion-weighting gradient pulses, the preparation interval could be used with a more symmetric and shorter timing to reduce T_2-related signal losses. However, to minimize the interval's duration the usage of bipolar diffusion-weighting gradient pulses with their improved efficiency is still recommended [13].

It should be noted that the gradient pulse duration δ'' according to Eqs. (5) and (8) can be very short and may not be compatible with the finite ramp time required to realize the high amplitudes usually desired for diffusion-weighting gradient pulses. In principle, the equations could be solved for a reduced amplitude of the short gradient pulses. However, because the ramp time again depends on the amplitude, this is expected to be quite tedious. Furthermore, the efficiency gain achieved for very short δ'' is marginal because the timing parameters are very close to the magic length case where the efficiency ratios approach 1 (see Fig. 1b). Thus, it can be recommended to use the conventional approach based on monopolar diffusion-weighting gradient pulses in this parameter range instead.

The presented modification considers different delay times at the begin and end of the readout interval, i.e. $\delta_1 \neq \delta_3$, to take the timing demands in imaging experiments into account. Thus, it extends a previously presented work with bipolar diffusion gradients which was limited to identical delay time [13]. The theoretical results described for the short-echo-train regime are more general but simplify to those presented in [13] for $\delta_1 = \delta_3$. The diffusion-weighting efficiency achievable with the current approach is increased compared to that with identical delay times. For instance, the *b* value obtained in Fig. 6a and b is about 30% larger than that achievable with the symmetric approach of [13] for identical echo times and gradient amplitudes (data not shown).

MAGSTE pulse sequences like the presented approach can be applied to reduce or compensate cross-terms related to any background gradients. However, it should be kept in mind that they were designed to deal with cross-terms of microscopic background gradients that vary within a voxel and, for instance, are caused by susceptibility differences on a microscopic level. If only macroscopic background gradients like magnetic field inhomogeneities are present that can be considered to be constant within each voxel, other compensation strategies may be appropriate. The most prominent is to take the geometric average of acquisitions performed with opposite polarities of the diffusion-weighting gradient pulses which is expected to reduce such cross-terms sufficiently for most applications.

Cross-terms of microscopic background gradients with the gradient pulses applied for spatial encoding or to spoil unwanted signal contributions, are more difficult to account for. They are independent from the diffusion-weighted preparation but vary with the imaging sequence used, e.g. they are generally less pronounced for (fast) spin-echo techniques. These cross-terms are hard to compensate completely, however, with a careful sequence design involving temporally close de- and rephasing (see Fig. 1g) and an appropriate choice of the gradient pulse polarities (e.g. the cross-term of the $\pi/2$ slice selection and rephasing gradient pulses in the preparation interval with a constant background gradient is expected to vanish if one of the combinations is inverted), these cross-terms can be minimized and are much smaller than those of non-compensated diffusion-weighting gradient pulses.

6. Conclusion

An extension of the generalized magic asymmetric gradient stimulated echo (generalized MAGSTE) sequence has been presented that involves bipolar diffusion-weighting gradient pulses, i.e. a third gradient pulse with inverted polarity is added to the readout and preparation interval. As for the underlying generalized MAGSTE sequence, the gradient pulse durations can be adjusted to compensate cross-terms with background gradients in the preparation and readout interval independently, but with bipolar gradients a higher diffusion-weighting efficiency can be achieved. Thus, the extension may help to improve the applicability of generalized MAGSTE.

Acknowledgment

Parts of this work were supported by Deutsche Forschungsgemeinschaft and Bundesministerium für Bildung und Forschung (Neuroimage Nord).

Appendix A

The derivation of Eqs. (5) and (8) is summarized in the following paragraphs. The cross-terms of Eqs. (4) and (7) are cubic polynomials of δ''. Their zero-crossings can be determined with the method of Cardano [20,21] which describes the solutions of the equation

$$c_3x^3 + c_2x^2 + c_1x + c_0 = 0 \tag{A.1}$$

depending on the coefficients c_i.

For the short-echo-train regime, i.e. Eq. (4),

$$4\,p^3 + 27\,q^2 < 0 \tag{A.2}$$

with

$$\begin{aligned} p &= \tfrac{3\,c_3\,c_1 - c_2^2}{3\,c_3^2} \\ q &= \tfrac{2\,c_2^3}{27\,c_3^3} - \tfrac{c_2\,c_1}{3\,c_3^2} + \tfrac{c_0}{c_3} \end{aligned} \tag{A.3}$$

is fulfilled which means that three real solutions exist. They are given by

$$\begin{aligned} x_1 &= -\sqrt{-\tfrac{4}{3}\,p}\,\cos\left(\tfrac{1}{3}\arccos\left(-\tfrac{q}{2}\sqrt{-\tfrac{27}{p^3}}\right) + \tfrac{\pi}{3}\right) - \tfrac{c_2}{3\,c_3} \\ x_2 &= \sqrt{-\tfrac{4}{3}\,p}\,\cos\left(\tfrac{1}{3}\arccos\left(-\tfrac{q}{2}\sqrt{-\tfrac{27}{p^3}}\right)\right) - \tfrac{c_2}{3\,c_3} \\ x_3 &= -\sqrt{-\tfrac{4}{3}\,p}\,\cos\left(\tfrac{1}{3}\arccos\left(-\tfrac{q}{2}\sqrt{-\tfrac{27}{p^3}}\right) - \tfrac{\pi}{3}\right) - \tfrac{c_2}{3\,c_3} \end{aligned} \tag{A.4}$$

where

$$\sqrt{-\frac{4}{3}\,p} = \sqrt{8}\,(\delta + \delta_1 + \delta_2), \tag{A.5}$$

the argument of the arccos is

$$-\frac{q}{2}\sqrt{-\frac{27}{p^3}} = -\frac{6\delta^3 + 12\delta^2\,(2\delta_1 + \delta_2) + 6\delta(5\delta_1^2 + 6\delta_1\delta_2 + \delta_2^2) + 12\delta_1\delta_2\,(2\delta_1 + \delta_2) + 11\delta_1^3 - \delta_3^3}{8\sqrt{2}(\delta + \delta_1 + \delta_2)^3}, \tag{A.6}$$

and the final summand

$$-\frac{c_2}{3\,c_3} = \delta + \delta_1 \tag{A.7}$$

However, it remains to clarify which, if any, of the solutions obeys the required boundary condition $0 < \delta'' < \delta$.

The argument of the arccos given in Eq. (A.4) is positive for any reasonable timing with $\delta_3 < \delta + \delta_1$. Thus, the arccos has values in $\left[0, \frac{\pi}{2}\right]$ and the argument of the cos-function is within $\left[-\frac{\pi}{3}, \frac{\pi}{3}\right]$ for all x_i in Eq. (A.4) which results in positive cos-values. The leading factor for x_2, given by Eq. (A.5), is positive as well. Thus, x_2 is larger than the final summand which is $\delta + \delta_1$ and it can be concluded that it is not a suitable solution.

For x_3 in Eq. (A.6), the argument of the cos must be in $\left[-\frac{\pi}{3}, -\frac{\pi}{6}\right]$ which corresponds to cos-values within $\left[\frac{1}{2}, \frac{\sqrt{3}}{2}\right]$. Considering that the leading factor is negative, the maximum value of x_3 is achieved for a cos-value of $\frac{1}{2}$ but yields $(1 - \sqrt{2})\,(\delta + \delta_1) - \sqrt{2}\,\delta_2$ which is negative. Consequently, x_3 is also not the desired solution.

x_1 increases with δ_3, has a zero-crossing for $\delta_3 = \delta_{3,\mathrm{magic}}$, and is positive for any $\delta_3 > \delta_{3,\mathrm{magic}}$ which is the boundary condition for the short-echo-train regime, i.e. $x_1 > 0$ within the short-echo-train regime. The maximum value of x_1 as a function of δ_3 that can be achieved in a real experiment is obtained for $\delta_3 = \delta + \delta_1$ and is equal to δ only for negative δ_2. For large δ_2 it is $\frac{\delta}{2}$, i.e. it can be concluded that $x_1 < \delta$ for $0 \leqslant \delta_2 < \infty$, i.e. any relevant timing.

For the long-echo-train regime, i.e. Eq. (7),

$$4\,p^3 + 27\,q^2 > 0 \tag{A.8}$$

which means that there is only one real solution which is given Eq. (8). It is negative for large δ_3, increases with decreasing δ_3, and has a single zero-crossing at $\delta_3 = \delta_{3,\mathrm{magic}}$. Thus, it is positive for $\delta_3 < \delta_{3,\mathrm{magic}}$ which is fulfilled for the long-echo-train regime.

It remains to check, whether this solution may exceed the upper limit for δ''_{long}, i.e. $\delta + \delta_1 - \delta_3$. Solving $\delta''_{\mathrm{long}} = \delta + \delta_1 - \delta_3$ for δ_3 yields

$$\delta_3 = \sqrt[3]{6\delta^3 + \delta_1^3 + 12\delta^2\,(\delta_1 + \delta_2) + 6\delta\,(\delta_1 + \delta_2)^2} \tag{A.9}$$

which is beyond the maximum value of $\delta + \delta_1$ for δ_3. Thus, δ''_{long} is a reasonable solution within the full long-echo-train regime.

Appendix B

In this section, the argumentation to prove the enhanced k efficiency for bipolar gradient pulses is sketched. In the short-echo-train regime, the ratio of the gradient integrals k obtained with bipolar and with monopolar diffusion-weighting gradient pulses is given by

$$\frac{k_{\mathrm{bip,short}}}{k_{\mathrm{mono}}} = \frac{\delta' + \delta'' - (\delta - \delta'')}{\delta\,(1 - |\eta|)} = \frac{2\delta'' + \delta_1 - \delta_3}{\delta\,(1 - |\eta|)} \tag{A.10}$$

with δ'' given by Eq. (5). The easiest way is to consider the δ_2 dependency of the k ratio. There are several solutions for δ_2 that yield a value of 1 for the ratio, i.e. equal k values for both preparations. Only one of these solutions,

$$(\delta_2)_1 = \frac{1}{6\,\delta}\sqrt{12\delta^4 + 36\delta^3\delta_1 + 36\delta^2\delta_1^2 + 6\delta\,(\delta_1^3 - \delta_3^3)} - 6\,\delta\,(\delta + \delta_1), \tag{A.11}$$

could be positive and is achieved if $\delta_3 = \delta_{3,\mathrm{magic}}$. Because $\delta_3 > \delta_{3,\mathrm{magic}}$ in this regime, δ_2 must be larger than $(\delta_2)_1$ according to Eq. (2). Because in this case, the limit of the k ratio for large δ is $\frac{5}{2} - 5\sqrt{2}\,\sin\left(\frac{1}{3}\arcsin\left(\frac{3}{8}\sqrt{2}\right)\right) \approx 1.19$, i.e. larger than 1, it can be concluded that the k ratio is larger than 1 within the full short-echo-train regime, i.e. bipolar diffusion-weighting gradient pulses yield an improved k efficiency.

For the long-echo-train regime, the k ratio is

$$\frac{k_{\mathrm{bip,long}}}{k_{\mathrm{mono}}} = \frac{\delta' - \delta'' - (\delta + \delta'')}{\delta\,(1 - |\eta|)} = \frac{\delta_1 - \delta_3 - 2\delta''}{\delta\,(1 - |\eta|)} \tag{A.12}$$

where δ'' given by Eq. (5). The argumentation is analogous to that of the short-echo-train regime. In this case, only one solution of δ_2 is found for equal k values but it is identical to $(\delta_2)_1$ of Eq. (A.11). Because $\delta_3 < \delta_{3,\mathrm{magic}}$ is valid here, the δ_2 must be smaller than $(\delta_2)_1$. Considering that the k ratio approaches zero for large δ_2, i.e. beyond $(\delta_2)_1$, it can be concluded that the ratio is larger than 1 for the long-echo-train regime as well.

Thus, equal efficiencies are only obtained if $\delta_3 = \delta_{3,\mathrm{magic}}$ for finite (and positive) δ and δ_i. Otherwise, i.e. within the full short- and long-echo-train regimes, a larger k value is achieved for bipolar diffusion-weighting gradient pulses.

Appendix C

For trapezoidal gradients with a ramp time t_{ramp}, Eqs. (6) and (9) must be extended to

$$\begin{aligned} &g_1\Big(-2\delta''^3 + 6\delta''^2\,(\delta + \delta_1) + 6\delta''\,((\delta + \delta_1 + 2\delta_2)^2 - 2\delta_2^2) - 10\delta^3 \\ &\quad - 6\delta^2\,(3\delta_1 + 4\delta_2) - 6\delta\,(\delta_1^2 + 4\delta_1\delta_2 + 2\delta_2^2) - t_{\mathrm{ramp}}^3 - 2t_{\mathrm{ramp}}^2\,(\delta'' - \delta) \\ &\quad - 3t_{\mathrm{ramp}}\,(\delta''^2 - 2\delta''\,(\delta + \delta_1) - 8\delta_1\delta_2 - 8\delta\delta_2 - 6\delta\delta_1 - 3\delta^2 - 2\delta_1^2 - 4\delta_2^2)\Big) \\ &= g_2\Big(2\delta''^3 - 6\delta''^2\,(\delta + \delta_1) - 6\delta''\Big((\delta + \delta_1 + 2\delta_2)^2 - 2\delta_2^2\Big) - 2\delta^3 \\ &\quad - 2\delta_1^3 + 2\delta_3^3 - 6\delta\delta_1\,(\delta + \delta_1) + 2t_{\mathrm{ramp}}^2\,(\delta_3 + 2\delta'' - 2\delta) \\ &\quad + t_{\mathrm{ramp}}\,(-3\delta''^2 + 6\delta''\,(\delta + \delta_1) - 3\,(\delta + \delta_1)^2 + 3\delta_3^2)\Big) \end{aligned} \tag{A.13}$$

and

$$\begin{aligned} & g_1\Big(-2\delta''^3+6\delta''^2(\delta+\delta_1)-6\delta''(\delta+\delta_1)^2) \\ & \quad -10\delta^3-6\delta^2(3\delta_1+4\delta_2)-6\delta(\delta_1^2+4\delta_1\delta_2+2\delta_2^2) \\ & \quad +2t_{\mathrm{ramp}}^2(\delta-\delta'')+t_{\mathrm{ramp}}(3(\delta-\delta'')^2+6\delta_1(\delta-\delta''))\Big) \\ & = g_2\Big(2\delta''^3-6\delta''^2(\delta+\delta_1)+6\delta''(\delta+\delta_1)^2) \\ & \quad -2\delta^3-2\delta_1^3+2\delta_3^3-6\delta\delta_1(\delta+\delta_1) \\ & \quad +t_{\mathrm{ramp}}^3+2t_{\mathrm{ramp}}^2(\delta''-\delta-\delta_1+\delta_3) \\ & \quad +3t_{\mathrm{ramp}}(\delta^2+\delta''^2+\delta_1^2+\delta_3^2-2\delta\delta''-2\delta_1\delta''-2\delta\delta_1)\Big), \end{aligned} \tag{A.14}$$

respectively.

Appendix D

Considering different fill times δ_2 and δ_2' prior to and after the refocusing RF pulse in the preparation interval, respectively, yields

$$\delta''_{\mathrm{short}}=\delta+\delta_1+2(\delta_2-\delta_2')-2\sqrt{2}(\delta+\delta_1+2\delta_2-\delta_2')\cos\left[\frac{\pi}{3}+\frac{1}{3}\arccos\left(\frac{A}{8\sqrt{2}(\delta+\delta_1+2\delta_2-\delta_2')^3}\right)\right] \tag{A.15}$$

for the short-echo-train regime with

$$\begin{aligned} A= \quad & 6\delta^3+11\delta_1^3-\delta_3^3 \\ & -9\delta_2'^3+81\delta_2^3-147\delta_2^2\delta_2'+75\delta_2\delta_2'^2 \\ & +24\delta^2\delta_1+30\delta\delta_1^2 \\ & +\delta^2(45\delta_2-33\delta_2')+\delta\left(45\delta_2'^2+111\delta_2^2\right) \\ & +\delta_1\left(39\delta_2'^2+123\delta_2^2\right)+\delta_1^2(63\delta_2-39\delta_2') \\ & +\delta\delta_1(114\delta_2-78\delta_2')-150\delta_2\delta_2'(\delta+\delta_1) \end{aligned} \tag{A.16}$$

and

$$\delta''_{\mathrm{long}}=\delta+\delta_1+\delta_2-\delta_2'-\frac{1}{2}\sqrt[3]{B} \tag{A.17}$$

with

$$\begin{aligned} B= & 4\delta_3^3+24\delta^3+4\delta_1^3+4\delta_2^3-4\delta_2'^3+12\delta_2'^2(\delta+\delta_1+\delta_2) \\ & +12\delta_2^2(\delta-\delta_2')+12\delta^2(4\delta_1+5\delta_2-\delta_2') \\ & +12\delta_1^2(\delta_2-\delta_2')-24\delta\delta_2'(\delta_1+\delta_2)-24\delta\delta_2(3\delta_1+\delta_2') \end{aligned} \tag{A.18}$$

for the long-echo-train regime, respectively. Note that the timing is reversed in the readout interval, i.e. δ_2 is the fill time after, δ_2' that prior to the refocusing RF pulse.

References

[1] E.O. Stejskal, J.E. Tanner, Spin diffusion measurements: spin echoes in the presence of a time-dependent field gradient, J. Chem. Phys. 42 (1965) 288–292.
[2] W.S. Price, Pulsed field gradient nuclear magnetic resonance as a tool for studying translational diffusion: Part I. Basic theory, Concepts Magn. Reson. 9 (1997) 299–336.
[3] W.S. Price, Pulsed field gradient nuclear magnetic resonance as a tool for studying translational diffusion: Part II. Experimental aspects, Concepts Magn. Reson. A 10 (1998) 197–237.
[4] J. Zhong, R.P. Kennan, J.C. Gore, Effects of susceptibility variations on NMR measurements of diffusion, J. Magn. Reson. 95 (1991) 133–139.
[5] G. Zheng, W.S. Price, Suppression of background gradients in (B0 gradient-based) NMR diffusion experiments, Concepts Magn. Reson. A 30 (2007) 261–277.
[6] R.F. Karlicek Jr., I.J. Lowe, A modified pulsed gradient technique for measuring diffusion in the presence of large background gradients, J. Magn. Reson. 37 (1980) 75–91.
[7] R.M. Cotts, M.J.R. Hoch, T. Sun, J.T. Markert, Pulsed field gradient stimulated echo methods for improved NMR diffusion measurements in heterogeneous systems, J. Magn. Reson. 83 (1989) 252–266.
[8] J.G. Seland, G.H. Sørland, K. Zick, B. Hafskjold, Diffusion measurements at long observation times in the presence of spatially variable internal magnetic field gradients, J. Magn. Reson. 146 (2000) 14–19.
[9] P.Z. Sun, J.G. Seland, D. Cory, Background gradient suppression in pulsed gradient stimulated echo measurements, J. Magn. Reson. 161 (2003) 168–173.
[10] P.Z. Sun, A.S. Seth, J. Zhou, Analysis of the magic asymmetric gradient stimulated echo sequence with shaped gradients, J. Magn. Reson. 171 (2004) 324–329.
[11] P. Galvosas, F. Stallmach, J. Kärger, Background gradient suppression in stimulated echo NMR diffusion studies using magic pulsed field gradient ratios, J. Magn. Reson. 166 (2004) 164–173.
[12] P.Z. Sun, Improved diffusion measurement in heterogeneous systems using the magic asymmetric gradient stimulated echo (MAGSTE) technique, J. Magn. Reson. 187 (2007) 177–183.
[13] J. Finsterbusch, Improved diffusion-weighting efficiency of pulsed gradient stimulated echo MR measurements with background gradient cross-term suppression, J. Magn. Reson. 191 (2008) 282–290.
[14] J. Finsterbusch, Cross-term-compensated pulsed-gradient stimulated echo MR with asymmetric gradient pulse lengths, J. Magn. Reson. 193 (2008) 41–48.
[15] P. Mansfield, Multi-planar image formation using NMR spin echoes, J. Phys. C 10 (1977) 349–352.
[16] G. Zheng, W.S. Price, MAG-PGSTE: a new STE-based PGSE NMR sequence for the determination of diffusion in magnetically inhomogeneous samples, J. Magn. Reson. 195 (2008) 40–44.
[17] P.A. Bottomley, C.J. Hardy, Two-dimensional spatially selective spin inversion and spin-echo refocusing with a single nuclear magnetic resonance pulse, J. Appl. Phys. 62 (1987) 4284–4290.
[18] J. Pauly, D. Nishimura, A. Macovski, A k-space analysis of small-tip-angle excitations, J. Magn. Reson. 81 (1989) 43–56.
[19] C.J. Hardy, H.E. Cline, Spatial localization in two dimensions using NMR designer pulses, J. Magn. Reson. 82 (1989) 647–654.
[20] W.S. Anglin, J. Lambek, The heritage of Thales, Mathematics in the Renaissance, Springer-Verlag, New York, 1995. Chapter 24.
[21] I.N. Bronstein, K.A. Semendjajew, Taschenbuch der Mathematik, Nauka, Moscow and BSB B.G. Teubner Verlagsgesellschaft, Leipzig, 1985.
[22] H. Weingärtner, Self diffusion in liquid water. A reassessment, Z. Phys. Chem. 132 (1982) 129–149.